

PHOTOMETRYPIPELINE: An Automated Pipeline for Calibrated Photometry

Michael Mommert

Northern Arizona University, Department of Physics and Astronomy, Flagstaff, AZ 86011, USA

Abstract

PHOTOMETRYPIPELINE (PP) is an automated pipeline that produces calibrated photometry from imaging data through image registration, aperture photometry, photometric calibration, and target identification with only minimal human interaction. PP utilizes the widely used Source Extractor software for source identification and aperture photometry; SCAMP is used for image registration. Both image registration and photometric calibration are based on matching field stars with star catalogs, requiring catalog coverage of the respective field. A number of different astrometric and photometric catalogs can be queried online. Relying on a sufficient number of background stars for image registration and photometric calibration, PP is well-suited to analyze data from small to medium-sized telescopes. Calibrated magnitudes obtained by PP are typically accurate within ≤ 0.03 mag and astrometric accuracies are of the order of 0.3 arcsec relative to the catalogs used in the registration. The pipeline consists of an open-source software suite written in Python 2.7, can be run on Unix-based systems on a simple desktop machine, and is capable of realtime data analysis. PP has been developed for observations of moving targets, but can be used for analyzing point source observations of any kind.

Keywords: methods: data analysis, techniques: photometry, astrometry

1. Introduction

Telescopes across the globe acquire massive amounts of imaging data every night. While the underlying science goals vary widely in these observations — from deep observations of extragalactic targets to short observations of rapidly spinning asteroids — the immediate objective of most observations is similar: obtaining reliable and calibrated brightness measurements of usually faint point sources. This objective requires not only good seeing and transparency conditions, as well as more or less extensive planning in order to address the science goal in the most efficient way, but also a sophisticated and accurate reduction and analysis of the acquired data.

Large observatories often provide support in the reduction and analysis of their data. However, the majority of imaging data have been — and still is — acquired with telescope apertures of a few meters or smaller. Smaller telescopes are usually easier to access because they are more numerous, but the observer is often left alone in the data reduction and analysis process. This factor leads to large amounts of imaging data from smaller telescopes being left unanalyzed as their proper analysis is not considered worth the effort, or because observing conditions were not ideal. The availability of an automated and robust software pipeline to exploit these data would simplify access to this data treasure trove.

I present PHOTOMETRYPIPELINE (PP), a Python-based, open-source software suite that provides automated

and calibrated point-source photometry of imaging data, specifically designed for small to medium-sized telescopes. PP provides image registration, photometric analysis and calibration for both fixed and moving targets with only minimal user interaction. The pipeline can be run on Unix-based systems, ranging from desktop machine to larger and more capable machines. PP was originally designed to obtain photometry of asteroids, but can be applied to observations of any point-sources, including stars, extragalactic sources, artificial satellites, and space debris. Due to its modular and flexible design, it can be modified to work with data from nearly any professional telescope.

PP is available for download on GitHub¹. Since PP is still evolving, refer to the online documentation² for up-to-date information. This document describes the functionality of PP Version 1.0 as of 30 November 2016. Also refer to the documentation for installation guides and additional support.

2. Methods and Implementation

2.1. Overview

The pipeline is implemented as a suite of Python 2.7 scripts. It makes use of Python packages that are freely available and easy to install through the Python Package Index³; required packages include NumPy⁴, SciPy⁵, as-

¹<https://github.com/mommermi/photometrypipeline>

²<http://mommermi.github.io/pp/index.html>

³<https://pypi.python.org/pypi>

⁴<http://www.numpy.org/>

⁵<https://www.scipy.org/>

Email address: michael.mommert@nau.edu (Michael Mommert)

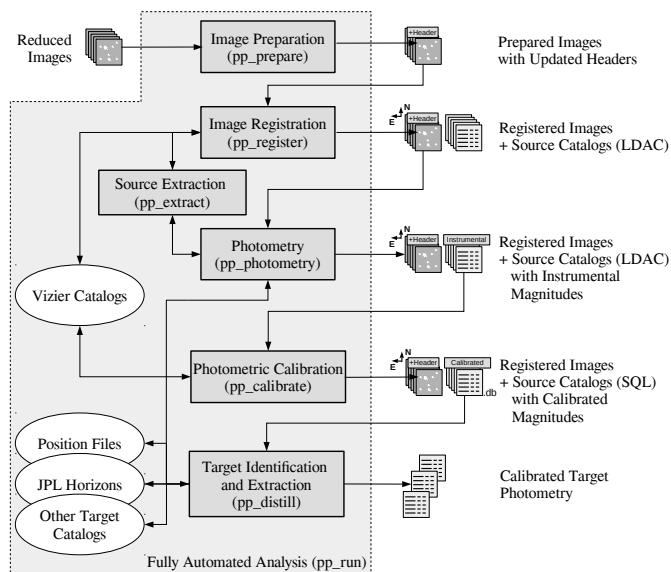


Figure 1: PP work flow diagram. The shaded area indicates the sequence of tasks run by the automatic analysis routine `pp_run`; the same sequence should be used if the individual tasks are run separately. White ovals indicate resources that are required in the analysis. The individual pipeline steps are discussed in Section 2.

ropy⁶, matplotlib⁷, and CALLHORIZONS⁸. For specific tasks, open-source software has been integrated into the pipeline. That software is called within the Python environment, but has to be installed on the machine prior to running the pipeline. The required auxiliary software is Source Extractor⁹ (Bertin and Arnouts, 1996) and SCAMP¹⁰ (Bertin et al., 2002), which are introduced below. Both Source Extractor and SCAMP are well-tested and widely used within the community, providing a robust foundation for the most important pipeline features.

PP consists of a number of stand-alone Python scripts that can be called separately, or can be run automatically. Figure 1 presents the work flow of the automated pipeline routine (`pp_run`). The same sequence should be used if the individual tasks are called separately in order to meet the respective file dependencies. `pp_run` is designed to run automatically on the majority of all data provided; this implies that it might not run successfully on non-ideal data (see Section 4.3 for a discussion). Running the individual pipeline tasks separately, using fine-tuned parameters differing from the defaults used by `pp_run`, might be necessary to improve the outcome for non-ideal datasets.

The runtime of the pipeline depends on a number of different parameters, including the memory and computing power of the machine, the image size, the number of images, the background star density, and the number and nature of targets in each field. For instance, running the ex-

ample data presented in Section 3 (79 700 pixel \times 700 pixel images, one target in the field) through the default pipeline (using `pp_run`) on a quad-core 1.9 GHz laptop running Ubuntu Linux 16.04 takes less than 20 minutes. With minor modifications, PP is able to provide real-time data analysis.

Every step of the image analysis process is thoroughly documented and summarized in a “diagnostics” HTML file that is created on-the-fly. This webpage allows for inspection of each pipeline process and serves as a validation of the data quality. Furthermore, it allows for identification of data affected by background sources, artifacts, and target mis-identification.

In order to provide the best possible results, PP should be run on fully reduced image data, which includes flat fielding and bias correction, as well as trimming of the data. It is mandatory that all frames coming from the same instrument have the same image dimensions.

2.2. Pipeline Tasks

The individual pipeline tasks shown in Figure 1 are described in detail below. Refer to the documentation provided online for more details on how to use these tasks.

2.2.1. Image Data Preparation – `pp_prepare`

In order to allow for the degree of automation provided by PP, it heavily relies on properly populated FITS image headers. Since every instrument/telescope combination uses slightly different formats, each combination has to be set up before data can be run through the pipeline. This setup consists of tailored parameter files for Source Extractor and SCAMP (see below), as well as a dictionary that translates header information into a format that is readable by the pipeline. In order to exploit its full potential, PP requires information on the telescope pointing and the date and time of the observations, as well as the detector pixel scale, detector binning, the official Minor Planet Center¹¹ (MPC) identifier of the observatory, the used photometric filter, and the target name to be present in each FITS image header.

Pipeline task `pp_prepare` identifies the used instrument and then reads, translates, and modifies the required FITS header keywords into a common format that is independent of the instrument and readable by all pipeline tasks. It also removes existing plate solutions in the World Coordinate System (WCS, see Greisen and Calabretta, 2002; Calabretta and Greisen, 2002) format from the header and implants a zero-th order solution based on the provided image coordinates, the detector pixel scale, and the typical image orientation for the respective telescope/instrument combination. This step is crucial for proper image registration (see Section 2.2.2).

This approach grants a high degree of flexibility to the pipeline, making it applicable to a large range of telescopes and instruments.

⁶<http://www.astropy.org/>

⁷<http://matplotlib.org/>

⁸<https://github.com/mommermi/callhorizons> and Section 5

⁹<http://www.astromatic.net/software/sextractor>

¹⁰<http://www.astromatic.net/software/scamp>

¹¹<http://minorplanetcenter.net>

2.2.2. Image Registration – `pp_extract` and `pp_register`

A plate solution for each input image is found using SCAMP, which computes astrometric solutions based on coarse WCS information in the FITS image header (provided by `pp_prepare`), a catalog of all sources in the field, and a reference catalog. SCAMP works completely automatic. Field source catalogs are generated using Source Extractor in the binary Leiden Data Analysis Center (LDAC) catalog format. Source Extractor identifies field sources based on their signal-to-noise ratio (SNR) and a minimum number of connected pixels that exceed that SNR threshold. For each source, Source Extractor provides the position in image and – if available – WCS coordinates, different flavors of photometry, descriptive flags, and other diagnostic parameters. Both Source Extractor and SCAMP are integrated into PP; the user will not have to interact with either of them directly.

Source extraction is performed by `pp_extract`, using Source Extractor, building a LDAC catalog for each input image. Source Extractor parameters can be controlled through `pp_extract`. In order to improve runtime and to exploit multi-CPU architecture, `pp_extract` uses Python’s multi-threading capabilities. Despite the fact that all pipeline results rely on this task, normally it will not be called by the user directly – although this is possible, and recommended in specific cases.

LDAC catalogs are read into `pp_register`, which calls SCAMP to find and imprint an astrometric solution into each image file. SCAMP matches LDAC catalogs against catalogs with astrometric solutions that it retrieves from the VizieR service¹² at the Centre de Données astronomiques de Strasbourg¹³. A large number of potential catalogs is available (refer to the SCAMP manual for an overview); PP usually utilizes URAT-1 (Zacharias et al., 2015), 2MASS (Skrutskie et al., 2006), or USNO-B1 (Monet et al., 2003), providing robust astrometry. `pp_register` will try each of the aforementioned catalogs (in that order) until all input images have been registered successfully. For each catalog, SCAMP is called twice using the same catalog, unless all input images have been registered successfully in the first run; the second run uses additional information created in the first SCAMP run. Registration fails if the number of field stars is too small (fewer than 10-20 stars), the images suffer from severe artifacts, or the initial WCS header solution is too far off (typically more than ~ 10 arcmin). Typically, image registration is successful even if the image orientation is previously unknown, given that the image center position and pixel scale are reasonably well known. The derived astrometric solution includes image distortion corrections as derived by SCAMP; the order of the correction terms varies for different telescopes. The results of `pp_register`, including information on each input image and a thumbnail image indicating the match based on the utilized catalog, are

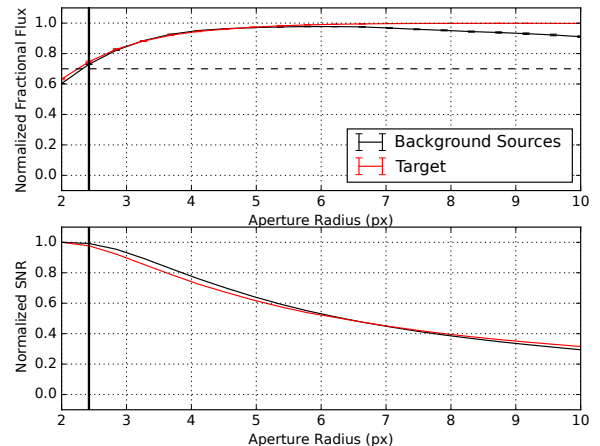


Figure 2: Curve-of-Growth diagnostic plot created by PP for one image from the data set used in Section 3. The top panel shows the normalized fractional flux of the target and the background sources as a function of aperture radius, the bottom panel shows the normalized SNR. The vertical bar indicates the aperture radius that is adopted as optimum aperture radius using the criteria discussed in Section 2.2.3.

added to the diagnostics webpage. The reliability of the image registration provided by SCAMP and PP is verified in Section 4.2.

2.2.3. Photometry – `pp_photometry`

PP uses aperture photometry performed by Source Extractor. The optimum aperture radius used in this process is derived in a curve-of-growth analysis (Howell, 2000), in which `pp_extract` measures the flux and its corresponding uncertainty for each source in every image using 20 different aperture radii. The target (or multiple targets) is identified (see Section 2.2.5) and its fluxes are isolated from those of the background sources. The fluxes for the target and the background sources are averaged separately over all images as a function of aperture radius and normalized separately. As shown in Figure 2, the normalized flux distribution and the SNR distribution have their maximum at different aperture radii. By increasing the aperture radius, more flux from each source is included; at the same time, the increase in aperture area also increases the noise contribution from the background. Hence, the flux is maximized at the largest aperture radius, but the SNR is maximized at a radius of typically 1.5 FWHM (Howell, 2000). In the case of moving target observations, the target or the background sources might be trailed, leading to additional difficulties.

PP uses by default the following criteria for the optimum aperture radius (compare to Figure 2): the smallest aperture radius at which at least 70% of each of the total target flux and the total background flux is included and at the same time the difference between the normalized target and background flux levels is smaller than 5%. These criteria make sure that trailing affects the target photom-

¹²<http://vizier.u-strasbg.fr/viz-bin/VizieR>

¹³<http://cds.u-strasbg.fr/>

etry at a level that is within the expected uncertainties of the photometry results. Alternatively, the user can select an aperture radius manually, or have the pipeline use that aperture radius that maximizes the SNR in the target or the background stars. Plots comparable to Figure 2 are generated on-the-fly for each image set processed by `pp-photometry` as part of the diagnostic output of the pipeline.

As a result of `pp-photometry`, LDAC catalogs for each input image are created that make use of the optimum (or manually selected) aperture radius; the catalogs contain instrumental magnitudes.

2.2.4. Photometric Calibration – `pp_calibrate`

PP provides photometric calibration of each image using background stars in the same field. The advantage of the photometric calibration using field stars is that data from different telescopes can be compared directly and that transparency and/or seeing variations can be compensated for.

In order to obtain calibrated photometry, the offset between the measured instrumental magnitudes and the respective photometric filter used in the observations – the magnitude zeropoint – has to be determined. In PP, this is done by comparing the brightness of field stars to their catalog brightness. Currently, PP supports the Sloan Digital Sky Survey Data Release 9 (SDSS-R9, Ahn et al., 2012, photometric bands: u, g, r, i, z) and the AAVSO Photometric All-Sky Survey Release 9 (APASS9, Henden et al., 2016, photometric bands: g, r, i, B, V) for optical bands, as well as 2MASS for the near-infrared bands (photometric bands: J, H, Ks), for calibration purposes.

Catalogs are queried from the VizieR service. In the case of optical data, SDSS is queried first; if there is no SDSS data available, APASS is used, which covers the majority of the Northern Hemisphere. Catalog data and field sources are matched based on astrometry; (near-) saturated or blended sources, as well as sources that do not have catalog counterparts, no or inaccurate ($\sigma > 0.05$ mag) photometric data are excluded from the following steps. The magnitude zeropoint (m_{zp}) of each frame is derived as follows (compare to Figure 3). The residual ζ_i between the catalog magnitude and the instrumental magnitude is calculated for all N available sources with index i . By minimizing

$$\chi^2 = \sum_i \frac{(m_{zp} - \zeta_i)^2}{\sigma_{\zeta,i}^2}, \quad (1)$$

the best-fit m_{zp} is determined, taking into account the uncertainties of the individual residuals, $\sigma_{\zeta,i}$, which are root-sum-squares of the uncertainties quoted in the catalogs and the instrumental uncertainties derived in the aperture photometry. Since some sources are affected by image artifacts or blending with background objects, their photometric measurements are compromised, leading to significantly increased residuals. In order to account for

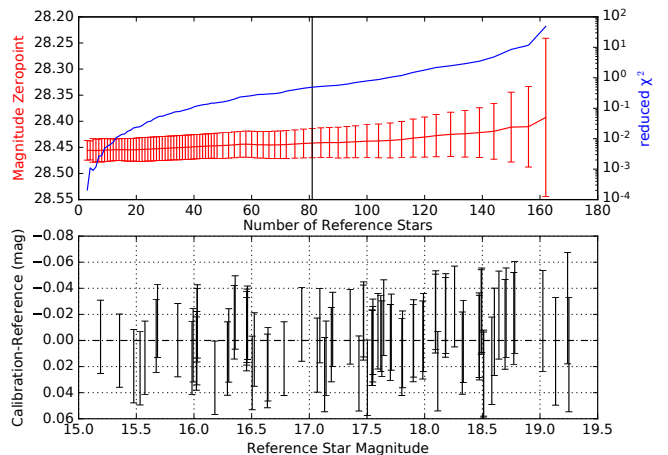


Figure 3: Photometric calibration diagnostic plot for one image from the data set used in Section 3. The top panel shows the derived magnitude zeropoint and according reduced χ^2 as a function of the number of reference stars used. The vertical line indicates the number of reference stars used in the final calibration. The bottom panel shows the residuals between the measured photometry in the image and the catalog magnitudes for this final calibration. Note that the zeropoint uncertainty is limited by the residual uncertainties – the final zeropoint uncertainty is 0.025 mag in this case. Also note that the zeropoint varies only insignificantly as a function of the number of reference stars.

these outliers, an iterative rejection scheme has been implemented that removes that source representing the largest outlier one at a time and recalculates the zeropoint magnitude after each rejection. The zeropoint magnitude featuring the minimum χ^2 of all iteration steps and at the same time having N equal at least 50% of the original number of sources is adopted. The threshold of 50% is somewhat arbitrary but generally leads to reliable results. The uncertainty associated with the magnitude zeropoint is determined as the quadratic sum of the average residual uncertainties and the weighted standard deviation of the residuals:

$$\sigma_{zp} = \sqrt{\frac{1}{N} \sum_i \sigma_{\zeta,i}^2 + \frac{1}{N} \sum_i \frac{(\zeta_i - m_{zp})^2}{\sigma_{\zeta,i}^2}} \quad (2)$$

Typical zeropoint magnitude uncertainties are of the order of 0.02–0.05 mag, based on typically ≥ 10 background sources. At least three sources are required for a photometric calibration; if no calibration is possible, instrumental magnitudes are reported. The reliability of the photometric calibration is verified in Section 4.1.

Final calibrated photometric measurements for all sources in each field are written into a queryable SQLite¹⁴ database. Plots similar to Figure 3 are generated for each input image as part of the diagnostic output.

PP supports transformations between photometric systems. Using equations provided by Chonis and Gaskell

¹⁴<https://sqlite.org/>

(2008), SDSS ugriz magnitudes can be transformed into BVRI magnitudes. Also, using Hodgkin et al. (2009), 2MASS near-infrared bands can be converted into the UKIRT system, which uses the standard Mauna Kea near-infrared filters. Uncertainties introduced through these transformations are typically of the order of a few 0.01 mag (see Section 4.1 for a discussion). Additional transformations and photometric catalogs will be implemented in the future.

Being designed for single-band data, PP does not support a color-term correction in addition to the derivation of the magnitude zeropoint. For observatories that automatically obtain data in different bands, such a correction could be implemented, potentially improving the overall photometric calibration quality.

2.2.5. Target Identification and Extraction – pp_distill

Photometry for selected targets is extracted from the SQLite databases using `pp_distill`. Targets are identified based on their WCS coordinates provided through simple text files, or manually provided fixed coordinates; ephemerides for moving targets are queried from JPL Horizons using the `CALLHORIZONS` Python module. Other types of target catalogs, e.g., through a query of SIMBAD¹⁵ or match with other online resources, will be implemented in the future.

For each target, a photometry file is generated that provides extensive information, as well as diagnostic output that allows to inspect the data quality. Furthermore, `pp_distill` automatically selects one reasonably bright star as “control star”, which is treated the exact same way as any other target and allows for an assessment of the reliability of the entire analysis procedure.

2.2.6. Data Products

The final data products of the pipeline include (1) SQLite database files with positions, calibrated magnitudes, and additional information on each source detected for each input frame, (2) ASCII tables with extracted information on each target that has been identified, and (3) a summary website with the combined diagnostic output of each pipeline task.

3. Example Results

In order to test the reliability of the pipeline, PP is run over V band imaging data of asteroid (2704) Julian Loewe taken with Lowell Observatory’s 42-inch telescope (Oszkiewicz et al., 2016) and compared to results derived with the commercial MPO Canopus¹⁶ software. MPO Canopus also provides astrometric and photometric calibration of imaging data. In the case of this data set, the photometric calibration provided by MPO Canopus is based on a

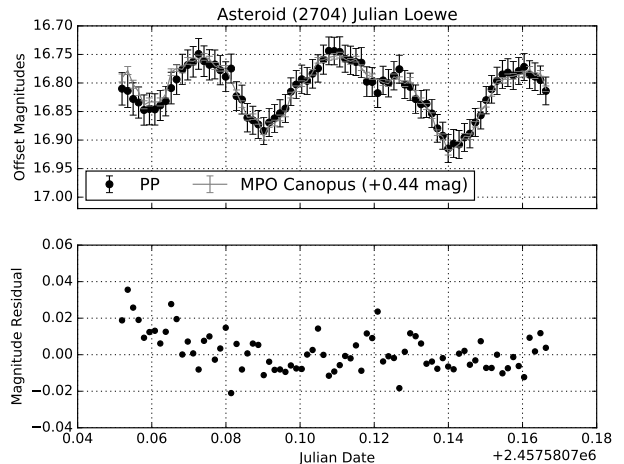


Figure 4: Optical (V band) lightcurve of asteroid (2704) Julian Loewe as measured by PP and the commercial MPO Canopus software (top panel). The relative agreement between both lightcurves is excellent (0.01 mag standard deviation of the residuals, lower panel). A constant offset between both lightcurve measurements of 0.44 mag is found (see text).

transformation from 2MASS near-infrared magnitudes to optical magnitudes (Binzel, 2004) due to a lack of other calibration stars.

The resulting lightcurve from PP and the comparison to the MPO Canopus results are displayed in Figure 4. The relative agreement between the lightcurves obtained by the programs is excellent. The standard deviation of the residuals between both data sets is of the order of 0.01 mag, which is smaller than the uncertainties provided by PP and of the same magnitude as the uncertainties provided by MPO Canopus. Note, however, that there is a constant offset between the reported magnitudes of 0.44 mag. This offset is most likely a result of the 2MASS-based photometric calibration of MPO Canopus: while optical magnitudes are affected by galactic extinction, this is not the case in the near-infrared bands provided by 2MASS. Furthermore, this method explicitly assumes that all near-infrared magnitudes unambiguously extrapolate to optical magnitudes. Hence, a constant offset between the two data analyses has to be expected.

4. Discussion

Section 3 proves the robustness of PP results in comparison to other available software. The following sections prove the claimed photometric and astrometric accuracy of the pipeline.

4.1. Photometric Accuracy

The photometric calibration accuracy provided by PP is verified using observations of standard star fields and their photometry from the literature. This experiment

¹⁵<http://simbad.u-strasbg.fr/simbad/>

¹⁶<http://www.minorplanetobserver.com/MP0Software/MP0Canopus.htm>

Field	N	SDSS-R9 Residuals	APASS9 Residuals
RU149	399	0.019±0.024* (0.039)	-0.014±0.023 (0.036)
PG0231+051	20	0.002±0.018 (0.025)	-0.005±0.014 (0.036)
PG1047+003	24	0.019±0.025 (0.032)	-0.009±0.025 (0.050)
PG1323-086	18	—	0.020±0.027 (0.065)
95-142	30	0.013±0.025 (0.025)	0.001±0.025 (0.043)
95-43	27	0.013±0.021 (0.033)	-0.001±0.023 (0.035)

Table 1: Verification of the photometric accuracy. N is the number of stars in the respective field, the residual columns list the mean and the standard deviation of the residuals between the values provided by P. Stetson and the measured magnitudes based on the respective catalog with PP; numbers in brackets are the default 1σ uncertainties on the magnitude zeropoint as derived by PP. Residual means and standard deviations are better than 0.03 mag, reflecting the overall calibration accuracy that can be achieved with the pipeline using available catalogs. (*: SDSS-R9 photometry compromised due to nonuniform coverage of SDSS-R9 stars throughout the field.)

uses observations of 5 different standard star fields (centered on 95-43, 95-142, PG0231+051, PG1047+003, PG1323-086, and RU149) taken with the Discovery Channel Telescope and its Large Monolithic Imager (LMI, Massey et al., 2013) in the V band. PP is run over the LMI data automatically (using `pp_run`) and with its default settings; the stars are unambiguously identified based on finder charts and their positions. The resulting calibrated photometry, based on the SDSS-R9 and APASS9 catalogs, is compared to values measured by Stetson (2000)¹⁷. Table 1 compiles the mean photometric residuals and the standard deviations of the residuals measured per field. Since the instrumental uncertainties for the stars are small (≤ 0.01 mag), the residual statistics reflect the calibration accuracy of the pipeline. For all fields, the standard deviation is larger than the mean residual for both catalogs, suggesting that any systematic offsets are statistically insignificant. Both SDSS-R9 and APASS9 provide magnitude zeropoints that are accurate within ≤ 0.03 mag (1σ level), using the default pipeline settings. PP 1σ uncertainties are consistently larger than the sample standard deviations, proving the conservative nature of the default pipeline uncertainties. Johnson–Cousins V magnitudes are transformed from SDSS g and r magnitudes (see Section 2.2.4).

Manual interaction, e.g., decreasing the aperture radius or reducing/increasing the number of stars used in the photometric calibration procedure can improve the overall photometric accuracy. Also, the future availability of high quality photometric catalogs, e.g., provided by Pan-STARRS, GAIA, LSST, will further improve the accuracy of the photometric calibration.

4.2. Astrometric Accuracy

Proper astrometric calibration is necessary for unambiguous target identification, but also provides crucial orbital information for asteroids and positional information

Field		Positional Residuals (arcsec)		
		URAT-1	2MASS	USNO-B1
RU149	RA	0.0±0.4 (503)	0.0±0.4 (488)	0.0±0.5 (487)
	Dec	0.0±0.2 (503)	0.0±0.3 (488)	0.0±0.4 (487)
PG0231+051	RA	0.0±0.1 (39)	0.1±0.3 (51)	0.1±0.2 (53)
	Dec	0.0±0.1 (39)	-0.1±0.3 (51)	0.0±0.4 (53)
PG1047+003	RA	0.0±0.1 (44)	0.0±0.3 (43)	-0.1±0.4 (42)
	Dec	0.0±0.1 (44)	0.0±0.2 (43)	0.1±0.7 (42)
PG1323-086	RA	0.0±0.1 (54)	0.0±0.3 (53)	0.0±0.3 (53)
	Dec	0.0±0.2 (54)	0.0±0.3 (53)	0.0±0.3 (53)
95-142	RA	0.0±0.2 (46)	0.0±0.2 (47)	0.1±0.3 (43)
	Dec	0.0±0.1 (46)	0.0±0.3 (47)	-0.1±0.3 (43)
95-43	RA	0.0±0.1 (32)	0.0±0.2 (31)	0.1±0.2 (32)
	Dec	0.0±0.1 (32)	0.0±0.3 (31)	-0.1±0.3 (32)

Table 2: Verification of the astrometric accuracy. Mean positional residuals and corresponding standard deviations based on comparing stars’ positions from registered images and their catalogued positions; numbers in brackets are the number of stars used in the comparison.

for other targets. PP relies on SCAMP and available catalogs to establish plate solutions and astrometric calibration; currently available catalogs are URAT-1, 2MASS, and USNO-B1. This implies that PP is subject to the same systematic and statistical offsets that are inherent to each of these catalogs. For a discussion of these intrinsic offsets, please refer to the corresponding catalog publications.

In order to quantify the astrometric uncertainty introduced by PP, the positions of stars found in the image data used in Section 4.1 are compared to the catalog positions. Each field is registered using different catalogs and the residuals in RA and Dec are derived relative to those catalogs. Results are shown in Table 2. Mean residuals are typically zero with standard deviations ≤ 0.3 arcsec. Star positions from the images and the catalogs have been matched within 5 arcsec in order to minimize the number of false pairs. However, a few matches still have residuals of a few arcsec, artificially increasing the standard deviations. Generally, the URAT-1 catalog provides more accurate positions than the other two catalogs. This is most likely due to the fact that it is the most recently published catalog relative to the date the image data have been taken, minimizing the stars’ proper motions.

The astrometric uncertainty introduced by PP is typically of the order of 0.3 arcsec, depending on the utilized catalog, which allows for accurate positional measurements of the targets. Note that positions measured from images use Source Extractor’s windowed centroids (XWIN_WORLD, YWIN_WORLD, see Source Extractor Manual) that use a weighting scheme and provide positional precision similar to PSF fitting routines.

4.3. Limitations of the Pipeline

PP has been designed to provide reliable photometric measurements for the majority of imaging data taken with a large range of different telescopes/instruments. This implies that PP will require manual adjustments – or fail entirely – in a small fraction of possible applications. The

¹⁷www.cadca-ccda.hia-ihh.nrc-cnrc.gc.ca/en/community/STETSON/standards

success of PP depends largely on the availability of non-saturated background stars for the image registration and photometric calibration. Hence, data taken with extraordinarily short integration times, small fields of view, or under bad transparency conditions might require manual interaction or fail entirely.

Furthermore, the pipeline relies on the availability of astrometric and photometric catalogs to provide reliable and accurate results. Current catalogs cover most of the Northern Hemisphere, defining the application area of PP on the sky. The astrometric and photometric accuracy provided by the pipeline is mainly a function of the intrinsic accuracy of the catalogs used. The availability of high-accuracy catalogs in the near future (Pan-STARRS, Gaia, LSST) will also improve the accuracy provided by PP.

PP was not designed to provide high-accuracy photometry such as might be required for detecting exoplanet transits. Instead, the main objective of the pipeline is to provide reliable and calibrated photometry on the ≤ 0.03 mag level for targets that are bright enough.

4.4. Future Developments

The PP source code is maintained regularly, which includes the implementation of newly available catalogs, as well as the setup of additional telescope/instrument combinations. The pipeline is able to support data from basically all professional and some high-level amateur telescopes that are able to provide the necessary header information, including date and time of observation, as well as telescope pointing information. Future catalogs that will be supported by PP include GAIA, Pan-STARRS, and LSST data for highly improved astrometric and photometric calibration and a better sky coverage. Additional transformations between different photometric systems will be provided, as well.

Future releases of PP will also include additional support for observations of a wide range of targets of interest. Calibrated databases extracted from the FITS images can be matched with manually created target catalogs or online resources (e.g., SIMBAD). The output for each target can be submitted to large Virtual Observatory databases for public access. Improved manual target selection based directly on image coordinates will allow for the extraction of moving targets even from data for which astrometric calibration is impossible, e.g., through a lack of background stars, or significantly trailed stars. This will enable observations of uncatalogued objects and objects with large positional uncertainties, including satellites, space debris, and not-yet confirmed near-Earth asteroids.

By utilizing SWARP¹⁸ (Bertin, 2006), PP will be able to stack images based on WCS coordinates – also for moving targets. The stacking greatly improves the signal-to-noise ratio of the target.

Finally, PP will enable the identification and photometric measurement of serendipitously observed asteroids in each field. The astrometric accuracy of positions measured with the pipeline – especially in combination with catalogs as provided by GAIA – will greatly improve asteroid orbits at no additional cost. In addition to that, calibrated photometric measurements will supplement pointed asteroid observations and support efforts to find asteroid shapes and rotational periods (see, e.g., Āurech et al., 2015).

PP was initially developed in the framework of the “Mission Accessible Near-Earth Object Survey” (MANOS) and is supported by NASA NEO/SSO grants NNX14AN-82G (MANOS; PI, N. Moskovitz, Lowell Observatory) and NNX15AE90G (Rapid response observations of NEOs, PI: D. E. Trilling, Northern Arizona University). The author would like to thank N. Moskovitz for numerous discussions and testing the pipeline in its different development stages, P. Massey for providing the Discovery Channel Telescope LMI data of standard fields, B. Skiff for useful discussions and analyzing the observations of asteroid 2704 with MPO Canopus, D. Oszkiewicz for permission to use this data set here, and D. E. Trilling for suggestions on the manuscript. The author would also like to thank E. Bertin and the Astrometric team for providing their software to the public. Finally, the author would like to thank an anonymous referee for useful suggestions and comments that improved this manuscript.

5. Appendix: CALLHORIZONS – A Python Module to query JPL Horizons

PP was originally designed for the analysis of asteroid observations and therefore depends on ephemerides in order to properly identify asteroids in the image data. These ephemerides are obtained from the JPL Horizons system (Giorgini et al., 1996), providing an accurate and reliable source of Solar System ephemerides. Horizons can be manually queried through a web interface¹⁹ or a telnet interface.

In order to be able to query ephemerides for a large number of asteroids and dates into a Python environment, I created CALLHORIZONS²⁰. This Python module allows to query Horizons using its web interface in order to obtain ephemerides and orbital elements for given dates or date ranges. All objects in the Horizons database can be queried, including planets, asteroids, comets, and spacecraft. The query results are provided as NumPy arrays, providing a large degree of flexibility in the analysis. Also, CALLHORIZONS provides a direct interface to the PyEphem module²¹: orbital elements queried by CALLHORIZONS

¹⁹<http://ssd.jpl.nasa.gov/horizons.cgi>

²⁰<https://github.com/mommermi/callhorizons>

²¹<http://rhodesmill.org/pyephem/>

¹⁸<http://www.astromatic.net/software/scamp>

can be directly turned into PyEphem objects, enabling the user to calculate ephemerides locally.

References

- Ahn, C.P., Alexandroff, R., Allende Prieto, C., Anderson, S.F., Anderton, T., Andrews, B.H., Aubourg, É., Bailey, S., Balbinot, E., Barnes, R., et al., 2012. The Ninth Data Release of the Sloan Digital Sky Survey: First Spectroscopic Data from the SDSS-III Baryon Oscillation Spectroscopic Survey. *ApJS* 203, 21. doi:10.1088/0067-0049/203/2/21, arXiv:1207.7137.
- Bertin, E., 2006. Automatic Astrometric and Photometric Calibration with SCAMP, in: Gabriel, C., Arviset, C., Ponz, D., Enrique, S. (Eds.), *Astronomical Data Analysis Software and Systems XV*, p. 112.
- Bertin, E., Arnouts, S., 1996. SExtractor: Software for source extraction. *A&AS* 117, 393–404. doi:10.1051/aas:1996164.
- Bertin, E., Mellier, Y., Radovich, M., Missonnier, G., Didelon, P., Morin, B., 2002. The TERAPIX Pipeline, in: Bohlender, D.A., Durand, D., Handley, T.H. (Eds.), *Astronomical Data Analysis Software and Systems XI*, p. 228.
- Binzel, R.P., 2004. A Simplified Method for Standard Star Calibration. *Minor Planet Bulletin* 32, 93–95.
- Calabretta, M.R., Greisen, E.W., 2002. Representations of celestial coordinates in FITS. *A&A* 395, 1077–1122. doi:10.1051/0004-6361:20021327, arXiv:astro-ph/0207413.
- Chonis, T.S., Gaskell, C.M., 2008. Setting UBVRI Photometric Zero-Points Using Sloan Digital Sky Survey ugriz Magnitudes. *AJ* 135, 264–267. doi:10.1088/0004-6256/135/1/264, arXiv:0710.5801.
- Giorgini, J.D., Yeomans, D.K., Chamberlin, A.B., Chodas, P.W., Jacobson, R.A., Keesey, M.S., Lieske, J.H., Ostro, S.J., Standish, E.M., Wimberly, R.N., 1996. JPL's On-Line Solar System Data Service, in: *AAS/Division for Planetary Sciences Meeting Abstracts #28*, p. 1158.
- Greisen, E.W., Calabretta, M.R., 2002. Representations of world coordinates in FITS. *A&A* 395, 1061–1075. doi:10.1051/0004-6361:20021326, arXiv:astro-ph/0207407.
- Henden, A.A., Templeton, M., Terrell, D., Smith, T.C., Levine, S., Welch, D., 2016. VizieR Online Data Catalog: AAVSO Photometric All Sky Survey (APASS) DR9 (Henden+, 2016). *VizieR Online Data Catalog* 2336.
- Hodgkin, S.T., Irwin, M.J., Hewett, P.C., Warren, S.J., 2009. The UKIRT wide field camera ZYJHK photometric system: calibration from 2MASS. *MNRAS* 394, 675–692. doi:10.1111/j.1365-2966.2008.14387.x, arXiv:0812.3081.
- Howell, S.B., 2000. *Handbook of CCD Astronomy*. Cambridge University Press.
- Massey, P., Dunham, E.W., Bida, T.A., Collins, P., Hall, J.C., Hunter, D.A., Lauman, S., Levine, S., Neugent, K., Nye, R., Oliver, R., Schleicher, D., Zoonematkermani, S., 2013. As Big and As Good As It Gets: The Large Monolithic Imager for Lowell Observatory's 4.3-m Discovery Channel Telescope, in: *American Astronomical Society Meeting Abstracts #221*, p. 345.02.
- Monet, D.G., Levine, S.E., Canzian, B., Ables, H.D., Bird, A.R., Dahn, C.C., Guetter, H.H., Harris, H.C., Henden, A.A., Leggett, S.K., Levison, H.F., Luginbuhl, C.B., Martini, J., Monet, A.K.B., Munn, J.A., Pier, J.R., Rhodes, A.R., Rieke, B., Sell, S., Stone, R.C., Vrba, F.J., Walker, R.L., Westerhout, G., Brucato, R.J., Reid, I.N., Schoening, W., Hartley, M., Read, M.A., Tritton, S.B., 2003. The USNO-B Catalog. *AJ* 125, 984–993. doi:10.1086/345888, arXiv:astro-ph/0210694.
- Oszkiewicz, D., Skiff, B.A., Moskovitz, N., Kankiewicz, P., Marciniak, A., Licandro, J., Galiazzo, M., Zeilinger, W., 2016. Non-Vestoid candidate asteroids in the inner main belt. *ArXiv e-prints* arXiv:1612.07788.
- Skrutskie, M.F., Cutri, R.M., Stiening, R., Weinberg, M.D., Schneider, S., Carpenter, J.M., Beichman, C., Capps, R., Chester, T., Elias, J., Huchra, J., Liebert, J., Lonsdale, C., Monet, D.G., Price, S., Seitzer, P., Jarrett, T., Kirkpatrick, J.D., Gizis, J.E., Howard, E., Evans, T., Fowler, J., Fullmer, L., Hurt, R., Light, R., Kopan, E.L., Marsh, K.A., McCallon, H.L., Tam, R., Van Dyk, S., Wheelock, S., 2006. The Two Micron All Sky Survey (2MASS). *AJ* 131, 1163–1183. doi:10.1086/498708.
- Stetson, P.B., 2000. Homogeneous Photometry for Star Clusters and Resolved Galaxies. II. Photometric Standard Stars. *PASP* 112, 925–931. doi:10.1086/316595, arXiv:astro-ph/0004144.
- Đurech, J., Hanuš, J., Vančo, R., 2015. Asteroids@home-A BOINC distributed computing project for asteroid shape reconstruction. *Astronomy and Computing* 13, 80–84. doi:10.1016/j.ascom.2015.09.004, arXiv:1511.08640.
- Zacharias, N., Finch, C., Subasavage, J., Bredthauer, G., Crockett, C., Divittorio, M., Ferguson, E., Harris, F., Harris, H., Henden, A., Kilian, C., Munn, J., Rafferty, T., Rhodes, A., Schultheiss, M., Tilleman, T., Wieder, G., 2015. The First U.S. Naval Observatory Robotic Astrometric Telescope Catalog. *AJ* 150, 101. doi:10.1088/0004-6256/150/4/101, arXiv:1508.04637.